Korean J. Chem. Eng., 39(12), 3464-3472 (2022)
DOI: 10.1007/s11814-022-1242-9

pISSN: 0256-1115
eISSN: 1975-7220

Comprehensive evaluation of high-temperature sintering behavior of sea sand vanadia-titania magnetite based on grey relational analysis

Zhen-xing Xing*,, Zhuang Huang*,**, Gong-jin Cheng*,**, He Yang*,**, Xiang-xin Xue*,**,***,****,†, and Guo-dong Zhang*****,†**

*School of Metallurgy, Northeastern University, Shenyang 110819, P. R. China
**Liaoning Key Laboratory of Recycling Science for Metallurgical Resources, Shenyang 110819, P. R. China
***Northeastern University Innovation Research Institute of Vanadium and Titanium Resource Industry - Technology, Shenyang 110819, P. R. China
****Innovation Research Institute of Comprehensive Utilization Technology for Vanadium-Titanium Magnetite Resources in Liaoxi District, Chaoyang 122000, P. R. China
*****Chengde Jianlong Special Steel Co., Ltd.
(*Received 16 April 2022 • Revised 7 July 2022 • Accepted 26 July 2022*)

Abstract−Sea sand vanadia-titania magnetite is difficult to pelletize, and it is difficult for iron and steel enterprises to use it as a raw material for ironmaking. In this paper, the high-temperature physicochemical characteristics and sintering behavior of sea sand vanadia-titania magnetite were comprehensively studied and systematically evaluated. The high-temperature metallurgical physicochemical characteristics of different iron ore powders and under different experimental conditions were studied by the micro-sintering experimental system. The high-temperature sintering indexes were comprehensively evaluated by the grey correlation analysis, and the influence of sea sand ore on sintering performance was investigated by sintering pot experiment. The research results show that the high-temperature sintering characteristics of sea sand vanadia-titania magnetite were the worst, and the grey correlation degree was the lowest. The high-temperature sintering characteristics of sintered blocks with sea sand ore were affected by changing the basicity and the addition amount of sea sand ore. When the basicity was 0.8 and the addition amount of sea sand ore was 15 wt%, the evaluation index of grey relational analysis was the best. The vertical sintering speed and tumble index were slightly reduced by adding sea sand ore, but the sinter yield was improved and the particle size distribution of sinter was optimized. The experimental results provide a certain data reference for the actual production of sinter with sea sand vanadia-titania magnetite.

Keywords: High-temperature Physicochemical Characteristics, Sea Sand Vanadia-titania Magnetite, Sintering Behavior, Grey Relational Analysis, Comprehensive Evaluation

INTRODUCTION

With the rapid development of the iron and steel industry, the demand for iron ore has increased rapidly. However, the high-quality iron ore resources gradually decrease, and the price of raw materials such as iron ore increases, forcing iron and steel enterprises to make use of vanadia-titania magnetite resources in order to reduce the production cost of enterprises [1]. Vanadia-titania magnetite is a kind of multi-symbiotic iron ore mainly composed of iron, accompanied by vanadia-titania and various valuable elements (such as chromium, cobalt, nickel, scandium), and it is also a kind of mineral resource with large reserves and wide distribution [2]. Different types of vanadia-titania magnetite resources have been found all over the world. China is the first country in the world to realize blast furnace smelting of vanadia-titania magnetite [3].

Sea sand vanadia-titania magnetite is a complex iron ore resource with titanomagnetite as the main ore phase formed by erosion. There are deposits distributed in Japan, Philippines, Indonesia, Australia, New Zealand, and the coastal areas of Hainan Island in China, which are rich in reserves, easy to mine and low in price [4-8]. Sea sand vanadia-titania magnetite is regular particle shaped, with smooth and dense surface, coarse particle size, small specific surface area, poor ball milling performance and pelletizing performance, and it is difficult to granulate in the process of pelletizing [9-11]. Therefore, it has not been used on a large scale as a raw material for ironmaking in iron and steel industry, and most of the related studies focus on the pre-oxidation treatment and reduction of sea sand raw ore [12-14].

Traditional sintering research mainly focuses on the normal temperature indicators such as chemical composition and physical properties. This evaluation method lacks comprehensive research on high-temperature metallurgical physicochemical properties of iron ore powder, so it is difficult to reasonably select and utilize various iron ore powders [15,16]. High-temperature sintering characteristics are an important high-temperature physicochemical property of iron ore powder. Different iron ore powders have different sintering behavior at high temperature. The sintering effect is related to the characteristics of various iron ore powders at high temperature [17-19]. Wu et al. [20-22] proposed the basic characteristics of

†To whom correspondence should be addressed.
E-mail: xuexx@mail.neu.edu.cn, zhangguodong@ejianlong.com

iron ore powder sintering and systematically studied the high-temperature physical and chemical properties of iron ore powder at high temperature, and provided a new idea for further optimizing the sintering process. Zhang et al. [23] studied the basic characteristics of Australian iron ore concentrate and its effects on sinter properties during a high-limonite sintering process by micro-sintering and sintering pot methods. Liu et al. [24,25] studied the effects of iron sand ratios on the basic characteristics of vanadium titanium mixed ores. The results show that the iron sand ratio in vanadium titanium mixed ores should be controlled within 9-12 wt%.

The above studies mainly focus on the characterization of the high-temperature sintering characteristics of single iron ore powder, and there are few optimization studies and comprehensive evaluations on the high-temperature metallurgical physicochemical characteristics of different basicity and mixed iron ore powders. In this study, the high-temperature metallurgical physicochemical characteristics of single and mixed iron ore powders were investigated by micro-sintering experiment, and the high-temperature metallurgical physicochemical characteristics and sintering behavior of different basicity and mixed iron ore powders were comprehensively evaluated by the grey relational analysis method. At the same time, the effect of sea sand ore on the properties of sinter was explored by sintering pot experiment.

MATERIALS AND METHODS

1. Experimental Materials

The raw materials used in this experiment mainly include New Zealand Sea sand ore (HS), Yuantong-14 (YT-14), Sijiaying (SJY), PB powder and lime. The experimental raw materials were quantitatively analyzed by ICPAES (Optima 8300DV; PerkinElmer, USA) and XRF (ZSXPrimus-II; Rigaku, Japan). The results are shown in Table 1. It can be seen that the total iron content of sea sand ore is 58.36 wt%, the content of TiO_2 and V_2O_5 is 6.95 wt% and 0.47 wt%, respectively, which belongs to a typical vanadia-titania magnetite. Yuantong-14 (YT-14) has the highest total iron content of 66.27 wt%, and the content of TiO_2 and V_2O_5 is 2.48 wt% and 0.29 wt%, respectively, which belongs to a kind of vanadia-titania iron ore powder. The total iron content of Sijiaying (SJY) and PB power is 65.29 wt% and 61.76 wt% respectively, containing less TiO_2 and V_2O_5, which can be regarded as ordinary iron ore powder.

2. Characteristic Analysis of Raw Materials

XRD (X'Pert Pro; PANalytical, Almelo, The Netherlands) was used to analyze the phase composition of the raw materials, and the results are shown in Fig. 1(a). Sea sand vanadia-titania magnetite is mainly composed of hematite (Fe_2O_3), magnetite (Fe_3O_4) and ilmenite spinel (Fe_2TiO_4). Titanium is mainly present in sea sand ore in the form of ilmenite spinel. The macroscopic morphology of the dried sea sand ore is shown in Fig. 1(b), and its microscopic morphology is shown in Fig. 1(c). It can be seen from Fig. 1 that the shape of sea sand ore particles is relatively regular, showing a spherical or ellipsoidal shape, the texture of the particles is smooth and shiny, and the density is relatively high. These characteristics are not conducive to the pelletizing process of sea sand ore.

The particle size distribution of the four main iron ore powders was analyzed by a vibrating screen, and the results are shown in

Table 1. Chemical composition of experimental raw materials (wt%)

Compositoins	TFe	FeO	SiO_2	CaO	MgO	Al_2O_3	TiO_2	V_2O_5
HS	58.36	28.23	3.27	1.15	2.88	3.33	6.95	0.47
YT-14	66.27	24.77	1.83	0.69	0.88	1.41	2.48	0.29
SJY	65.29	17.99	6.72	0.22	0.42	0.42	0.12	0.03
PB	61.76	21.45	3.66	0.32	0.32	1.96	0.43	0.02
Lime	-	-	1.97	54.13	2.67	1.08	-	-

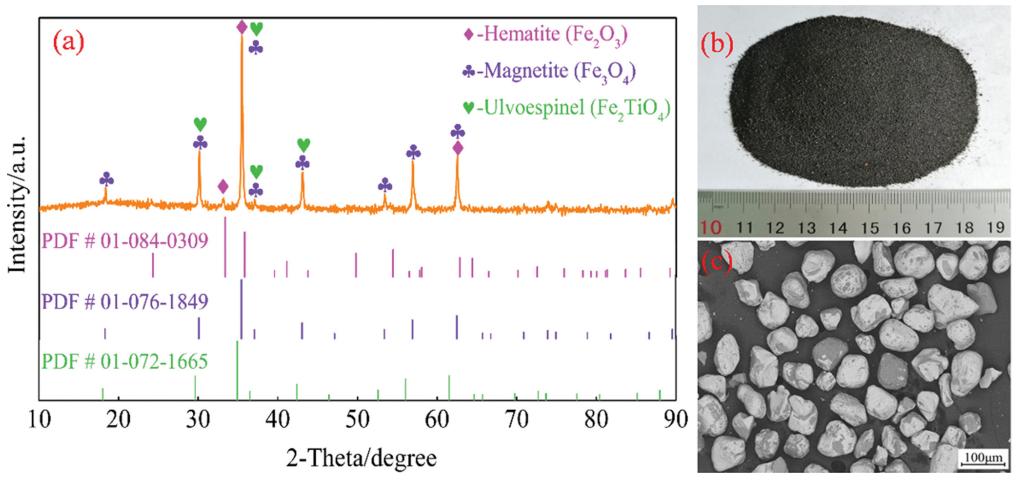

Fig. 1. The X-ray diffraction analysis diagram and morphology of sea sand ore. (a) XRD analysis diagram, (b) macroscopic morphology, (c) microscopic morphology.

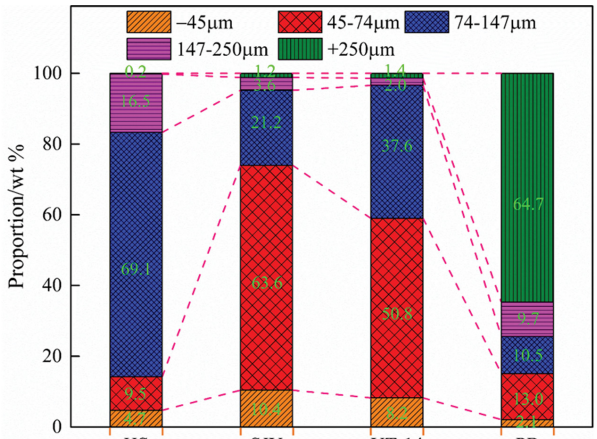

	HS	SJY	YT-14	PB
−45μm	4.7	10.4	8.2	2.1
45-74	9.5	63.6	50.8	13.0
74-147	69.1	21.2	37.6	10.5
147-250	16.5	3.6	2.0	9.7
+250μm	0.2	1.2	1.4	64.7

Fig. 2. The particle size distribution diagram of experimental raw materials.

Fig. 2. It can be seen from the particle size distribution diagram that PB powder is iron ore powder with relatively coarse particles, and 64.7 wt% of the particles are above 250 μm. The particle size of sea sand ore is also relatively coarse, and 69.1 wt% of sea sand ore is distributed in 74-147 μm. The particle size of SJY and YT-14 ores is relatively fine, and the proportion of particles with a particle size distribution of 45-74 μm is 63.6 wt% and 50.8 wt%, respectively.

3. Experimental Methods

The micro-sintering method is a micro-experiment that qualitatively simulates the physical and chemical changes of minerals and the formation of sintering liquid phase in the high-temperature sintering process of iron ore powder. Infrared heating is adopted in the process of high-temperature sintering experiment, so the sample does not need to add fuel. Fig. 3 shows the flow chart of the high-temperature sintering experiment, which mainly includes sample preparation (Fig. 3(a)), high-temperature sintering (Fig. 3(b)) and performance testing (Fig. 3(d), (e) and (f)). The high-temperature metallurgical physicochemical characteristics measuring system (RHL-45) of iron ore powder used in this experiment is shown in Fig. 3(b), and Fig. 3(c) shows the temperature heating curve in the high-temperature sintering process.

Fig. 3(d) shows the detection method of assimilation temperature; the assimilation temperature (AT) refers to the reaction ability of iron ore powder with CaO in the sintering process, which represents the difficulty of iron ore powder to form liquid phase in the sintering process [15,16]. Fig. 3(e) shows the detection method of liquid liquidity index; the liquid phase fluidity index (LF) refers to the fluidity of the liquid phase generated by the reaction between iron ore powder and CaO in the sintering process, which represents the effective bonding range of the binder phase [26,27]. The calculation formula of fluidity index is shown in Eq. (1).

$$\text{Liquid phase fluidity index (LF)} = \frac{S_{after} - S_{before}}{S_{before}} \quad (1)$$

where S_{before} is the vertical projection area of the adhering fines cylinder before the test (mm^2); S_{after} is the vertical projection area of melt after test (mm^2).

Fig. 3(f) shows the detection method of binder phase strength and intergranular consolidation strength; the binder phase strength (BS) represents the effective consolidation ability of the binder phase formed in the sintering process of iron ore powder to its surrounding iron ore particles [28]. The intergranular consolidation strength

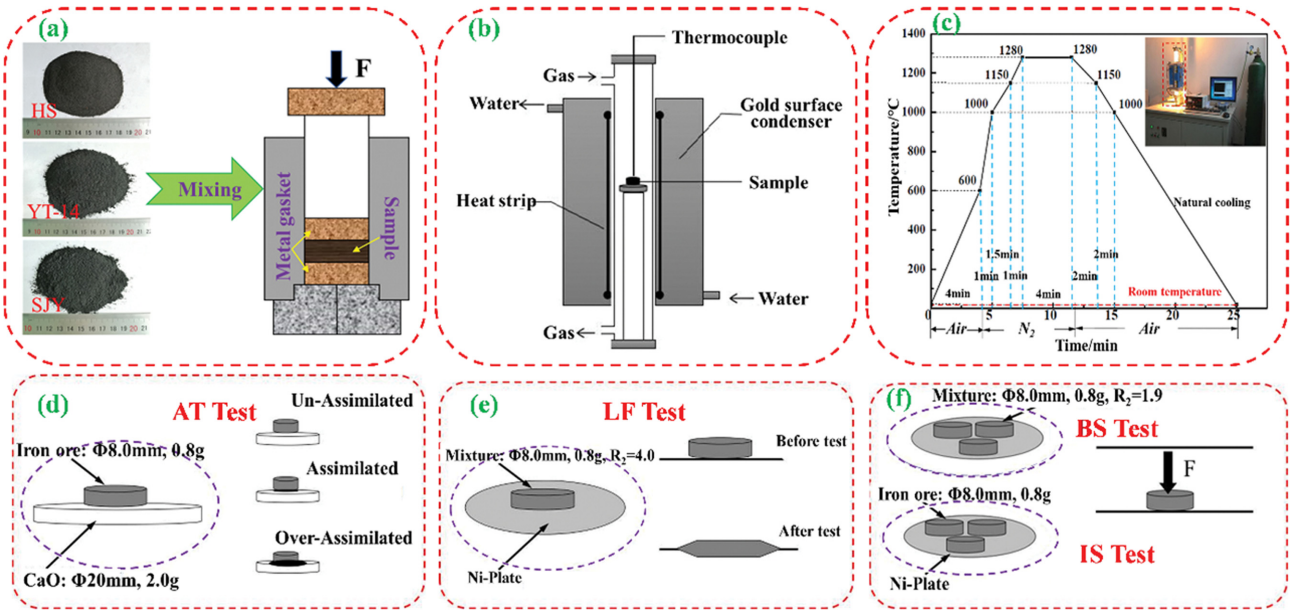

Fig. 3. Flow chart of high-temperature sintering experiment. (a) Sample preparation; (b) Experimental equipment; (c) Heating curve; (d) AT Test; (e) LF Test; (f) BS Test and IS Test.

Table 2. The high temperature sintering characteristics of experimental materials

Materials	AT/°C	LF/-	BS/N	IS/N
Sea sand ore	1,290	0.00	145	132
Yuantong-14	1,280	0.00	3,969	6,219
Sijiaying ore	1,230	0.52	2,178	3,783
PB powder	1,240	0.12	991	540

(IS) represents the ability of minerals formed by intergranular consolidation under the high-temperature state of the sintering process, whose indexes are expressed in the form of compressive strength of sintered block [29,30].

RESULTS AND DISCUSSION

1. High-temperature Sintering Characteristics of Sea Sand Ore

Based on the particularity of chemical composition and particle morphology of sea sand vanadia-titania magnetite, the high-temperature sintering characteristics of four iron ore powders, such as assimilation temperature (AT), liquid phase fluidity index (LF), binder phase strength (BS) and intergranular consolidation strength (IS), were studied by micro-sintering experiment. The experimental results are shown in Table 2.

It can be seen from the data in the Table 2 that the assimilation temperature of sea sand vanadia-titania magnetite was relatively high, which was 1,290 °C, indicating that it was difficult to form low melting point liquid phase when the sea sand ore reacted with CaO in the sintering process. The liquid phase fluidity index was almost 0.00, which indicated that the fluidity of liquid phase formed by sea sand ore and CaO in the sintering process was poor, which was not conducive to improving the consolidation strength of sinter. The binder phase strength of sea sand ore was low, which was 145 N, which indicated that the liquid phase formed in the high-temperature sintering process of sea sand ore had a poor consolidation strength to surrounding particles. The intergranular consolidation strength of sea sand ore was also low, only 132 N, which indicated that the strength of sea sand ore particles obtained by crystal bond connection in the sintering process was poor.

The YT-14 ore had the highest binder phase strength and intergranular consolidation strength, 3,969 N and 6,219 N, respectively. Followed by SJY ore, 2,178 N and 3,783 N, respectively. The various indicators of PB powder were general, among which the binder phase strength and intergranular consolidation strength were 991 N and 540 N, respectively.

2. Effect of Basicity on High-temperature Sintering Characteristics of Sea Sand Ore

According to the high-temperature sintering characteristics of sea sand ore, its assimilation temperature was high and its liquid phase fluidity was poor. Therefore, the effect of basicity (R_2=CaO wt%/MgO wt%) on the high-temperature sintering characteristics of sea sand ore was explored by adding lime. The results are shown in Fig. 4.

The experimental results show that with the increase of binary basicity, the assimilation temperature of sea sand ore was basically maintained at 1,310 °C, the liquid phase fluidity index increased gradually, the binder phase strength decreased gradually, and the intergranular consolidation strength increased first and then decreased. When the binary basicity was 1.0, the maximum intergranular consolidation strength was 10,155 N, the binder phase strength was still 3,830 N, the assimilation temperature was 1,310 °C, and the liquid phase fluidity was 0.0934. Therefore, the binary basicity should be controlled at about 1.0 in the sintering process of sea sand ore.

3. Effect of Sea Sand Dosage on High-temperature Sintering Characteristics

To explore the optimal dosage of sea sand ore in the sintering process, the experimental conditions were set as 51 wt% PB powder, 10 wt% ludwigite, the binary basicity was 1.0, and the addition amount of sea sand ore and Yuantong-14 ore was changed. The high-temperature sintering characteristics of sea sand ore were studied by micro sintering experiment. The effect of sea sand ore dosage on high-temperature sintering characteristics is shown in Fig. 5.

The experimental results show that with the addition amount of sea sand ore gradually increased from 5 wt% to 35 wt%, the assimilation temperature of sinter was maintained at 1,300 °C, while the liquid phase fluidity index, binder phase strength and intergranular consolidation strength all show a trend of first increasing and then decreasing. When the addition amount of sea sand ore was 15 wt%, the liquid phase fluidity index and the intergranular

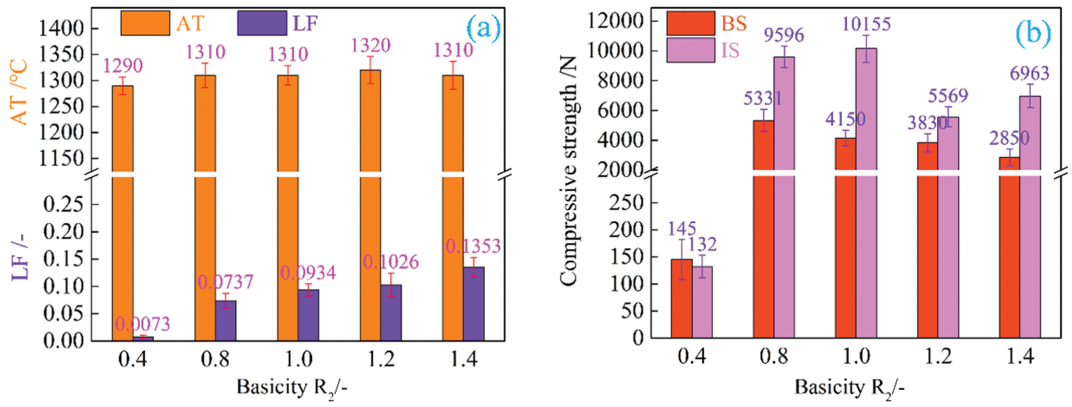

Fig. 4. Effect of limestone dosage on high-temperature sintering characteristics of sea sand ore. (a) AF and LF; (b) BS and IS.

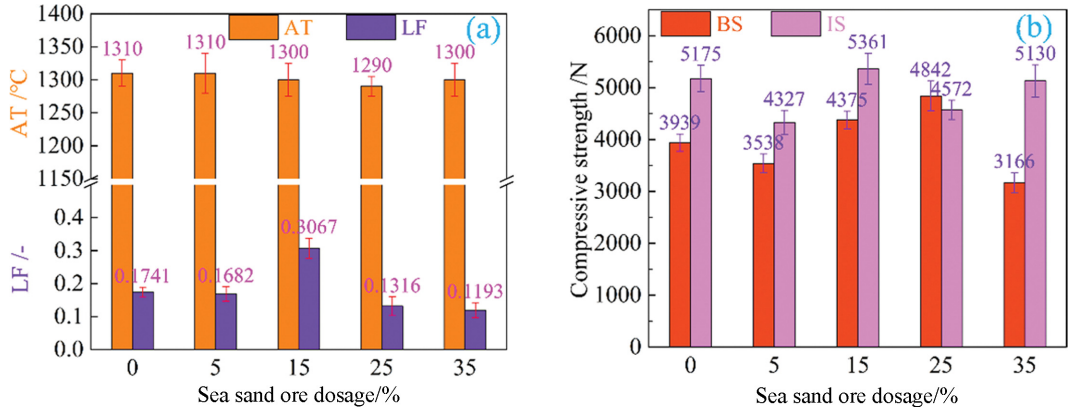

Fig. 5. Effect of sea sand ore dosage on high-temperature sintering characteristics. (a) AF and LF; (b) BS and IS.

consolidation strength reached the maximum, 0.3067 and 5,361 N, respectively. The maximum value of the binder phase strength was 4,842 N, and the addition amount of sea sand ore was 25 wt%. When the added amount of sea sand ore was 35 wt%, the various indexes of high-temperature sintering characteristics showed a downward trend, but they were still in the appropriate range. Therefore, the appropriate dosage of sea sand ore in the sintering process should be 15-35 wt%, but subsequent sintering pot experiments should be carried out on this basis to further verify the appropriate dosage of sea sand ore.

4. Comprehensive Evaluation of High-temperature Sintering Characteristics of Sea Sand Ore

The high-temperature sintering characteristics of sea sand ore have certain differences under different experimental conditions. To explore the correlation degree between the high-temperature sintering indexes under different experimental conditions, grey correlation degree analysis was introduced to comprehensively evaluate the high-temperature sintering indexes under different experimental conditions. The grey system theory proposes the concept of grey correlation analysis of each subsystem, which aims to find the numerical relationship between the various factors in the system through a certain method. Therefore, the quality of the high-temperature sintering index can be evaluated by the value of the gray correlation degree.

Liu et al. [24,25] comprehensively evaluated the sintering basic characteristics of iron ore by gray relationship analysis. Qie et al. [31] studied the optimal sintering basic characteristic index of mixed ore under the condition of high limonite ratio. Wang et al. [32] proposed a decision model of the priority sequence for mineral resources development and utilization based on the grey relational analysis method. The above research results show that the effect of comprehensive evaluation by grey correlation analysis is good. In the analysis process, the high-temperature sintering indexes obtained from four kinds of iron ore powder, different basicity and sea sand ore dosage are taken as three independent evaluation systems, respectively. The calculation steps of grey correlation degree are as follows.

4-1. Reference Sequence and Comparison Sequence

The high-temperature sintering index under different experimental conditions is regarded as the element of matrix, which is called comparison sequence. When evaluating four kinds of iron ore fines, the comparison sequence is $X_t=(X_1, X_2, X_3, X_4)$; when evaluating different basicity, the comparison sequence is $Y_t=(Y_1, Y_2, Y_3, Y_4, Y_5)$; when evaluating different sea sand ore dosages, the comparison sequence is $Z_t=(Z_1, Z_2, Z_3, Z_4, Z_5)$. The optimal value of each index was selected as the element of the reference sequence. The research shows that each high-temperature sintering index of iron ore has a certain reasonable range. Among them, the suitable ranges of assimilation temperature and liquid phase fluidity index are 1,275-1,315 °C and 0.7-1.6, respectively, and the binder phase strength and intergranular consolidation strength should be kept as high as possible [33]. Therefore, in the reference sequence, the average value of assimilation temperature and liquid phase fluidity index in the appropriate range is taken as the optimal value, and the maximum values of binder phase strength and intergranular consolidation strength in the above three independent systems are taken as the optimal value. Three matrices composed of reference sequence and comparison sequence can be obtained.

$$(X_0, X_1, X_2, X_3, X_4)=\begin{bmatrix} 1{,}295 & 1.15 & 3{,}969 & 6{,}219 \\ 1{,}290 & 0.00 & 145 & 132 \\ 1{,}280 & 0.00 & 3{,}969 & 6{,}219 \\ 1{,}230 & 0.52 & 2{,}178 & 3{,}783 \\ 1{,}240 & 0.12 & 991 & 540 \end{bmatrix}$$

$$(Y_0, Y_1, Y_2, Y_3, Y_4, Y_5)=\begin{bmatrix} 1{,}298 & 1.1500 & 5{,}331 & 10{,}155 \\ 1{,}290 & 0.0000 & 145 & 132 \\ 1{,}310 & 0.0737 & 5{,}331 & 9{,}596 \\ 1{,}310 & 0.0934 & 4{,}150 & 10{,}155 \\ 1{,}320 & 0.1026 & 3{,}830 & 5{,}569 \\ 1{,}310 & 0.1353 & 2{,}850 & 6{,}963 \end{bmatrix}$$

$$(Z_0, Z_1, Z_2, Z_3, Z_4, Z_5)=\begin{bmatrix} 1{,}295 & 1.1500 & 4{,}842 & 5{,}361 \\ 1{,}310 & 0.1741 & 3{,}939 & 5{,}175 \\ 1{,}310 & 0.1682 & 3{,}538 & 4{,}327 \\ 1{,}300 & 0.3067 & 4{,}375 & 5{,}361 \\ 1{,}290 & 0.1316 & 4{,}842 & 4{,}572 \\ 1{,}300 & 0.1193 & 3{,}166 & 5{,}130 \end{bmatrix}$$

4-2. Data Dimensionless Processing

Due to the different physical meanings of various factors in the

system, the dimensions of the data are not necessarily the same, resulting in no comparability between the evaluation indicators, or it is difficult to obtain correct conclusions during comparison. Therefore, it is generally necessary to carry out data dimensionless processing in the gray correlation analysis. The commonly used method is the averaging calculation method, as shown in Eq. (2), where i=0, 1, 2, 3, …, n; k=1, 2, 3, …, m. The new matrix is as follows:

$$x'_i(k)=\frac{x_i(k)}{\frac{1}{m}\Sigma_{k=1}^{m}x_i(k)} \tag{2}$$

$$(X'_0, X'_1, X'_2, X'_3, X'_4)=\begin{bmatrix} 0.451056 & 0.000401 & 1.382427 & 2.166116 \\ 3.292916 & 0.000000 & 0.370134 & 0.336950 \\ 0.446460 & 0.000000 & 1.384374 & 2.169166 \\ 0.684139 & 0.000289 & 1.211427 & 2.104145 \\ 1.789890 & 0.000173 & 1.430469 & 0.779468 \end{bmatrix}$$

$$(Y'_0, Y'_1, Y'_2, Y'_3, Y'_4, Y'_5)=\begin{bmatrix} 0.308661 & 0.000274 & 1.270636 & 2.420429 \\ 3.292916 & 0.000000 & 0.370134 & 0.336950 \\ 0.322718 & 0.000018 & 1.313291 & 2.363973 \\ 0.335573 & 0.000024 & 1.063074 & 2.601329 \\ 0.492579 & 0.000038 & 1.429224 & 2.078159 \\ 0.471090 & 0.000049 & 1.024891 & 2.503970 \end{bmatrix}$$

$$(Z'_0, Z'_1, Z'_2, Z'_3, Z'_4, Z'_5)=\begin{bmatrix} 0.450468 & 0.000400 & 1.684298 & 1.864833 \\ 0.502678 & 0.000067 & 1.511487 & 1.985769 \\ 0.571107 & 0.000073 & 1.542424 & 1.886396 \\ 0.471172 & 0.000111 & 1.585675 & 1.943041 \\ 0.482057 & 0.000049 & 1.809395 & 1.708499 \\ 0.541886 & 0.000050 & 1.319700 & 2.138364 \end{bmatrix}$$

4-3. Calculation of Difference Sequences

The sequence composed of the absolute value of the difference between the normalized reference sequence and the comparison sequence is called the difference sequence, expressed as $\Delta X'_{0i}(k)=|X'_0(k)-X'_i(k)|$. The results are as follows:

$$(\Delta X'_{01}, \Delta X'_{02}, \Delta X'_{03}, \Delta X'_{04})=\begin{bmatrix} 2.841860 & 0.000401 & 1.012293 & 1.829166 \\ 0.004597 & 0.000401 & 0.001947 & 0.003050 \\ 0.233083 & 0.000111 & 0.171000 & 0.061971 \\ 1.338834 & 0.000227 & 0.048041 & 1.386648 \end{bmatrix}$$

$$(\Delta Y'_{01}, \Delta Y'_{02}, \Delta Y'_{03}, \Delta Y'_{04}, \Delta Y'_{05})=\begin{bmatrix} 2.984255 & 0.000274 & 0.900502 & 2.083479 \\ 0.014057 & 0.000256 & 0.042655 & 0.056456 \\ 0.026911 & 0.000250 & 0.207562 & 0.180900 \\ 0.183917 & 0.000236 & 0.158588 & 0.342270 \\ 0.162429 & 0.000225 & 0.245745 & 0.083541 \end{bmatrix}$$

$$(\Delta Z'_{01}, \Delta Z'_{02}, \Delta Z'_{03}, \Delta Z'_{04}, \Delta Z'_{05})=\begin{bmatrix} 0.052210 & 0.000333 & 0.172812 & 0.120935 \\ 0.120639 & 0.000327 & 0.141874 & 0.021562 \\ 0.020704 & 0.000289 & 0.098623 & 0.078208 \\ 0.031589 & 0.000351 & 0.125096 & 0.156334 \\ 0.091418 & 0.000350 & 0.364598 & 0.273531 \end{bmatrix}$$

4-4. Calculation of Correlation Coefficient

According to the difference sequences of the above three independent systems, the maximum value ($\max_i \max_k |X'_0(k)-X'_i(k)|$) and the minimum value ($\min_i \min_k |X'_0(k)-X'_i(k)|$) of the difference sequence are selected, respectively. The calculation of correlation coefficient is shown in Eq. (3):

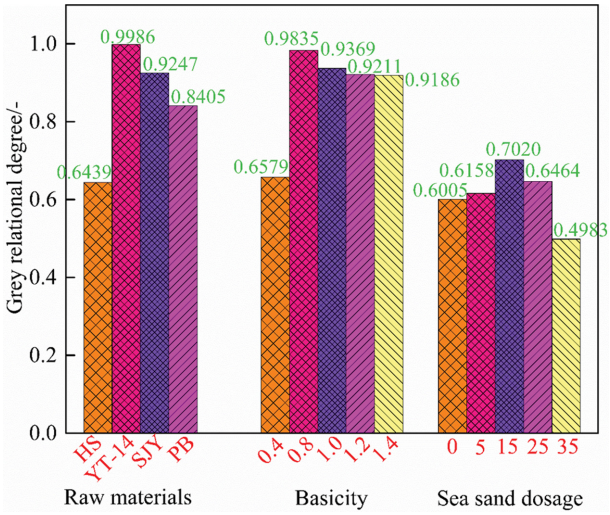

Fig. 6. Grey relational degree of different systems.

$$\xi_{0i}(k)=\frac{\min_i \min_k |X'_0(k)-X'_i(k)|+\rho \max_i \max_k |X'_0(k)-X'_i(k)|}{\Delta X'_{0i}(k)+\rho \max_i \max_k |X'_0(k)-X'_i(k)|} \tag{3}$$

where ρ is the differentiate coefficient, $\rho \in (0,1)$, which equals 0.5.

According to the calculation results of correlation coefficient, the correlation degree of each system can be calculated according to Eq. (4). The specific results are shown in Fig. 6.

$$r_t=\frac{\Sigma_{k=1}^{m}\xi_t(k)\omega_k}{\Sigma_{k=1}^{m}\omega_k} \tag{4}$$

where m is the number of elements in the sequence (k=0, 1, 2, …, m); $\xi_t(k)$ and ω_k are correlation coefficient and index weight, respectively. The weight values of assimilation temperature, liquid fluidity index, binder phase strength and intergranular consolidation strength were given as 0.2, 0.3, 0.4 and 0.1, respectively [24,25].

According to the grey correlation analysis results of the three independent systems in Fig. 6, the gray correlation degree order of the high-temperature sintering characteristics of the four iron ore powders was: HS<PB<SJY<YT-14. In the basicity variation system, with the increase of basicity, the comprehensive evaluation indexes of high-temperature sintering characteristics of sea sand ore showed a trend of first increasing and then decreasing. When the basicity was 0.8, the high-temperature sintering indexes of sea sand ore was the best. With the increase of sea sand ore dosage, the gray correlation degree of its high-temperature sintering characteristics first increased and then decreased. When the sea sand ore dosage was 5-25 wt%, the gray correlation degree was higher than that of the unadded sea sand ore, indicating that the sea sand ore dosage was the optimal amount.

5. Sintering Pot Experiment of Sea Sand Ore

To further explore the effect of sea sand ore on the properties of sinter, the sinter pot experiment of sea sand ore was carried out with a 700-mm deep×320-mm diameter sinter pot. Taking the actual production situation of the enterprise as a reference, calcium ash (CA) and magnesium ash (MA) were used to adjust the basicity (R_2=CaO wt%/MgO wt%), fixed carbon content (C wt%=4.5%).

Table 3. Sintering experimental scheme and mix proportion of sintering materials (wt%)

No.	HS	YT-14	OM[1]	RM[2]	MA[3]	CA[4]	R_2	Coal
1	0	23.5	35	30	3.3	8.2	2.15	4.5
2	5	18.5	35	30	3.1	8.4	2.15	4.5
3	5	3.5	50	30	3.2	8.3	2.15	4.5
4	5	3.5	50	30	2.3	9.2	2.30	4.5

[1]Ordinary magnetite; [2]Return mine; [3]Mg-Ash; [4]Ca-Ash.

Taking the basicity of sintered blocks and dosage of sea sand ore as variables, the effects of sea sand ore on vertical sintering speed, tumble index (TI), sinter yield and particle size distribution were studied. Because the actual production data of adding sea sand ore in sinter is less, and in order to ensure the successful operation of sintering pot experiment, only the sintering pot experiment with 5 wt% sea sand ore was carried out in this study. The specific experimental scheme is shown in Table 3, and the experimental parameters of the sintered pot are shown in Table 4.

The sintering pot test covered proportioning, mixing, pelletizing, feeding, ignition, sintering, crushing, and cooling. According to the recorded experiment data, the vertical sintering speed (Eq. (5)), sinter yield (Eq. (6)) and particle size distribution of sinter were calculated, and the tumble index (TI) measured in accordance with ISO 3271:2015 (Eq. (7)). The experimental results are shown in Fig. 7.

$$\text{Vertical sintering speed (mm/min)} = \frac{\text{Depth of sinter pot (mm)}}{\text{Sintering time (min)}} \quad (5)$$

$$\text{Yield (\%)} = \frac{\text{Mass of sinter above 5 mm (kg)} - \text{Mass of grate layer (kg)}}{\text{Mass of sinter all fractions (kg)} - \text{Mass of grate layer (kg)}} \times 100\% \quad (6)$$

$$\text{Tumble index (\%)} = \frac{\text{Mass of sinter above 6.3 mm after tumble (kg)}}{\text{Mass of sinter charged in tumble (kg)}} \times 100\% \quad (7)$$

According to the sintering experiment scheme (Table 3) and the quality index of sinter (Fig. 7), comparing No. 1 with No. 2 and No. 3, it can be found that the vertical sintering speed and tumble index of the sinter with 5 wt% sea sand ore were reduced, but the sinter yield increased. The sinter with a particle size of −5 mm decreased, medium-sized sinter increased, and the particle size distribution was more uniform. This is mainly because the sea sand ore is vanadia-titania magnetite containing V, Ti and other elements. The addition of sea sand ore led to the increase of TiO_2 content, an increase in the viscosity of the liquid phase in sinter, a decrease in the permeability of the material layer, and an increase in the resistance of the material layer. The increase of perovskite content with brittleness and high hardness resulted in a decrease in the vertical sintering speed and tumble index of the sinter [34]. However, adding the appropriate dosage of sea sand ore could also optimize the particle size distribution of the raw materials, which is conducive to the pelletizing in the sintering process. Thus, the sinter yield was improved to a certain extent.

Comparing No. 3 and No. 4, with the increase of basicity the tumble index of sinter increased, while the vertical sintering speed and yield decreased, but the particle size distribution of sinter changed little. This is mainly due to the increase of basicity, the increase of water consumption, and the lack of relative moisture in

Table 4. Parameters of sintering pot test

Item	Parameter	Item	Parameter
Pot height	700 mm	Pot diameter	320 mm
Sintering weight	100 kg	Height of grate layer	20 mm
Moisture	8.5±0.5 wt%	Pelletizing time	10 min
Ignition temperature	1,050 °C	Ignition time	2 min
Ignition pressure	8.0 kPa	Exhausting pressure	12.0 kPa

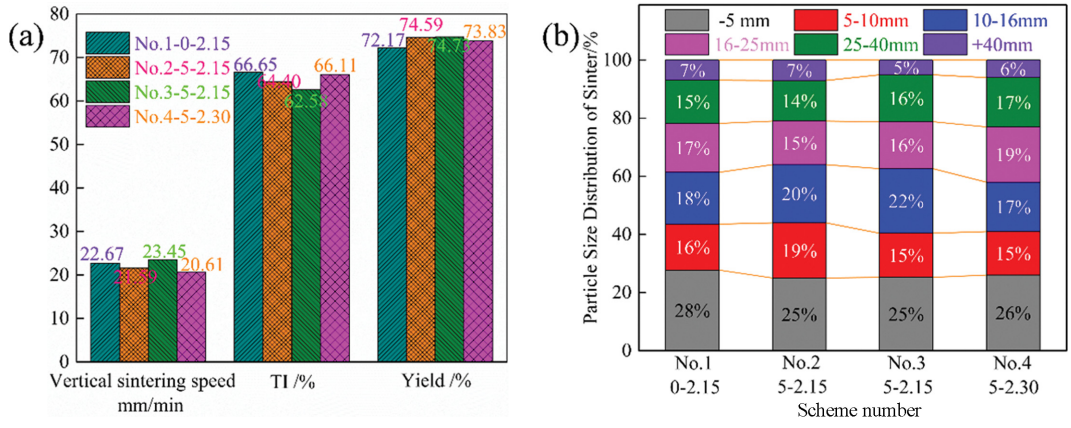

Fig. 7. Quality index and particle size distribution of sinter. (a) Vertical sintering speed, TI and Yield; (b) Particle size distribution of sinter.

pelletizing, which led to a decrease in the permeability of the material layer. Therefore, the vertical sintering speed and yield decreased slightly. In addition, with the increase of basicity, the content of calcium ferrite increased, which was beneficial to improving the tumble index of sinter [35,36]. Therefore, it can be considered to add an appropriate amount of sea sand ore in the sintering process. The research results provide a certain data reference for the actual production of sinter with sea sand ore.

CONCLUSIONS

The high-temperature metallurgical physicochemical characteristics and sintering behavior of sea sand ore under different experimental conditions were investigated, and high-temperature sintering behavior was comprehensively evaluated. The influence of sea sand ore on sinter properties was studied by sintering pot experiment.

1. The micro-sintering experiment results of iron ore powder show that the high-temperature sintering characteristics of sea sand ore were the worst. The assimilation temperature was the highest, reaching 1,290 °C, the liquid phase fluidity index was 0.00, and the binder phase strength and intergranular consolidation strength were the lowest, 145 N and 132 N, respectively.

2. When the basicity of sintered blocks with sea sand ore was changed by adding lime, the high-temperature sintering characteristics of sea sand ore were optimized to a certain extent, and the appropriate basicity should be controlled at about 1.0. The influence of different sea sand ore dosages on high-temperature sintering characteristics was different, and the appropriate proportion of sea sand ore should be 15-35 wt%.

3. The high-temperature sintering indexes obtained from four kinds of iron ore powder, different basicity and sea sand ore dosage were comprehensively evaluated by grey relational analysis. The results show that the gray correlation degree order of the high-temperature sintering characteristics of the four iron ore powders was: HS<PB<SJY<YT-14. When the basicity was 0.8 and the addition amount of sea sand ore was 15 wt%, the evaluation index of grey relational analysis was the best.

4. The experimental results of sea sand sintering pot show that the vertical sintering speed and tumble index were slightly reduced by adding the appropriate amount of sea sand ore, but the sinter yield was improved and the particle size distribution of sinter was optimized. The experimental results provide a certain data reference for the actual production of sinter with sea sand vanadia-titania magnetite.

ACKNOWLEDGEMENTS

The authors are especially thankful to the National Natural Science Foundation of China (Grant No.51674084, 21908020 and U1908226) and Fundamental Research Funds for the Central Universities (Grant No. N182503035).

DECLARATION OF COMPETING INTEREST

The authors report there are no competing interests to declare.

REFERENCES

1. G. J. Cheng, X. X. Xue, T. Jiang and P. N. Duan, *Metall. Mater. Trans. B*, **47**(3), 1713 (2016).
2. Y. N. Lu, S. L. Wu, H. Zhou, L. M. Ma, Z. J. Liu and Y. Wang, *ISIJ Int.*, **61**(8), 2211 (2021).
3. H. G. Du, *Principle of smelting vanadium-titanium magnetite in the blast furnace*, 1st ed., Science Press, Beijing, China (1996).
4. G. J. Cheng, Z. X. Xing, H. Yang and X. X. Xue, *Minerals*, **11**(1), 87 (2021).
5. J. B. Wright, *N.Z. J. Geol. Geophys.*, **10**(3), 659 (1967).
6. Z. X. Xing, G. J. Cheng, Z. X. Gao, H. Yang and X. X. Xue, *Metall. Res. Technol.*, **117**, 411 (2020).
7. Z. X. Xing, G. J. Cheng, H. Yang and X. X. Xue, *Experimental research on preparation of oxidized pellets with high proportion sea sand mine*, The 12th CSM Steel Congress, Beijing (2019).
8. Y. L. Qin, Q. F. Ling, K. Zhang and H. Liu, *Minerals*, **11**(8), 793 (2021).
9. Z. Wang, D. Pinson, S. Chew, H. Rogers, B. J. Monaghan, M. I. Pownceby, N. A. S. Webster and G. Q. Zhang, *Metall. Mater. Trans. B*, **47**, 330 (2016).
10. Z. X. Xing, G. J. Cheng, Z. X. Gao, H. Yang and X. X. Xue, *Metals*, **11**(2), 269 (2021).
11. A. Podder, *Trans. Indian Inst. Met.*, **74**(6), 1479 (2021).
12. E. Park and O. Ostrovski, *ISIJ Int.*, **44**, 74 (2004).
13. R. J. Longbottom, B. J. Monaghan and J. G. Mathieson, *ISIJ Int.*, **53**, 1152 (2013).
14. C. Geng, T. C. Sun, Y. W. Ma, C. Y. Xu and H. F. Yang, *J. Iron Steel Res. Int.*, **24**, 156 (2017).
15. S. L. Wu, Y. M. Dai, O. Dauter, Y. D. Pei, J. Xu and H. L. Han, *J. Univ. Sci. Technol. Beijing*, **32**(6), 719 (2010).
16. S. L. Wu, Y. Liu, J. X. Du, K. Mi and H. Lin, *J. Univ. Sci. Technol. Beijing*, **24**(3), 254 (2002).
17. H. Zhou, J. K. Wang, P. N. Ma, H. X. Meng, F. Z. Cheng and J. W. Luo, *J. Mater. Res. Technol.*, **15**, 4475 (2021).
18. M. X. Zhou and H. Zhou, *J. Mater. Res. Technol.*, **9**, 13106 (2020).
19. Y. X. Xue, J. Pan, D. Q. Zhu, Z. Q. Guo, C. C. Yang, L. M. Lu and H. Y. Tian, *Minerals*, **10**(9), 802 (2020).
20. S. L. Wu and G. L. Zhang, *Steel Research Int.*, **86**(9), 1014 (2015).
21. S. L. Wu, B. Su, Y. H. Qi, M. Y. Kou, Y. Li and W. L. Zhang, *Metall. Mater. Trans. B*, **48**(5), 2469 (2017).
22. X. B. Zhai, S. L. Wu, H. Zhou, L. X. Su and X. D. Ma, *Ironmak. & Steelmak.*, **47**(4), 405 (2020).
23. D. H. Liu, H. Liu, J. L. Zhang, Z. J. Liu, X. Xue, G. W. Wang and Q. F. Kang, *Int. J. Min. Met. Mater.*, **24**(9), 991 (2017).
24. D. H. Liu, J. H. Li, Y. Peng, J. L. Zhang, G. W. Wang and X. Xue, *J. Iron Steel Res. Int.*, **26**, 691 (2019).
25. D. H. Liu, J. L. Zhang, Z. J. Liu, Y. Z. Wang, X. Xue and J. Yan, *JOM*, **68**(9), 2418 (2016).
26. S. L. Wu, H. L. Han, H. X. Li, J. Xu, S. D. Yang and X. Q. Liu, *Int. J. Miner. Metall. Mater.*, **17**(1), 11 (2010).
27. G. L. Zhang, S. L. Wu, S. G. Chen, B. Su, Z. G. Que and C. G. Hou, *Int. J. Miner. Metall. Mater.*, **21**(10), 962 (2014).
28. G. J. Cheng, L. J. Li, X. X. Xue, H. Yang, W. J. Zhang and R. G. Bai, *J. Mater. Res. Technol.*, **17**, 2657 (2022).
29. J. L. Zhang, Z. W. Hu, H. B. Zuo, Z. J. Liu, Z. X. Zhao and T. J. Yang,

Ironmak. & Steelmak., **41**(4), 279 (2014).
30. H. He, X. Lv and J. Wang, *Mining Metall. & Explor.*, **38**, 2271 (2021).
31. Y. N. Qie, D. H. Liu, Q. Lv, X. J. Liu and Y. Q. Sun, *J. Iron Steel Res.*, **27**(9), 14 (2015).
32. Y. Wang, C. Zhang and G. P. Jiang, *Int. J. Min. Sci. Technol.*, **26**(3), 395 (2016).
33. G. L. Zhang, S. L. Wu, S. G. Chen, J. Zhu, J. X. Fan and B. Su, *ISIJ Int.*, **53**(9), 1515 (2013).
34. W. D. Tang, S. T. Yang, G. J. Cheng, Z. X. Gao, H. Yang and X. X. Xue, *Minerals*, **8**(7), 263 (2018).
35. S. T. Yang. M. Zhou, T. Jiang, Y. J. Wang and X. X. Xue, *T. Nonferr. Metal. Soc.*, **25**(6), 2087 (2015).
36. L. H. Zhang, Z. X. Gao, S. T. Yang, W. D. Tang and X. X. Xue, *Metals*, **10**(5), 569 (2020).